Redox Biology 43 (2021) 102004

Contents lists available at ScienceDirect

Redox Biology

journal homepage: www.elsevier.com/locate/redox

The histone methyltransferase SETD2 modulates oxidative stress to attenuate experimental colitis

Min Liu [a,b], Hanyu Rao [a,b], Jing Liu [a,b], Xiaoxue Li [a,b], Wenxin Feng [a,b], Liming Gui [a,b], Huayuan Tang [c], Jin Xu [b], Wei-Qiang Gao [a,b,*], Li Li [a,b,**]

[a] State Key Laboratory of Oncogenes and Related Genes, Renji-Med X Clinical Stem Cell Research Center, Ren Ji Hospital, School of Medicine and School of Biomedical Engineering, Shanghai Jiao Tong University, Shanghai, 200127, China
[b] School of Biomedical Engineering and Med-X Research Institute, Shanghai Jiao Tong University, Shanghai, China
[c] State Key Laboratory of Chemical Oncogenomics, School of Chemical Biology and Biotechnology, Peking University Shenzhen Graduate School, Shenzhen, China

ARTICLE INFO

Keywords:
IBD
SETD2
Oxidative stress
ROS
Epithelial barrier

ABSTRACT

Epigenetic regulation disorder is important in the onset and pathogenesis of inflammatory bowel disease (IBD). SETD2, a trimethyltransferase of histone H3K36, is frequently mutated in IBD samples with a high risk of developing colorectal cancer (CRC). However, functions of SETD2 in IBD and colitis-associated CRC remain largely undefined. Here, we found that SETD2 modulates oxidative stress to attenuate colonic inflammation and tumorigenesis in mice. SETD2 expression became decreased in IBD patients and dextran sodium sulfate (DSS)-induced colitic mice. *Setd2*$^{Vil\text{-}KO}$ mice showed increased susceptibility to DSS-induced colitis, accompanied by more severe epithelial barrier disruption and markedly increased intestinal permeability that subsequently facilitated inflammation-associated CRC. Mechanistically, we found that *Setd2* depletion resulted in excess reactive oxygen species (ROS) by directly down-regulating antioxidant genes, which led to defects in barrier integrity and subsequently inflammatory damage. Moreover, overexpression of antioxidant PRDX6 in *Setd2*$^{Vil\text{-}KO}$ intestinal epithelial cells (IECs) largely alleviated the overproductions of ROS and improved the cellular survival. Together, our findings highlight an epigenetic mechanism by which SETD2 modulates oxidative stress to regulate intestinal epithelial homeostasis and attenuate colonic inflammation and tumorigenesis. SETD2 might therefore be a pivotal regulator that maintains the homeostasis of the intestinal mucosal barrier.

1. Introduction

Inflammatory bowel disease (IBD) is a complex and relapsing inflammatory disorder that can be sub-classified into Crohn's disease (CD) and ulcerative colitis (UC) [1,2]. Chronic inflammation frequently leads to increased risk of tumorigenesis [3], and IBD patients have higher risk of colorectal cancer (CRC) development [4,5]. IBD results from a complex interactions between the mucosal barrier, commensal bacteria, and the immune system [6]. The intestinal mucosal barrier consists of intestinal epithelial cells (IECs), which are adhered to each other via intercellular junctions, and plays a critical role in protecting the gastrointestinal tract [7]. Defects in the barrier function allow the translocation of luminal pathogens and bacteria into the intestinal lamina propria and trigger chronic inflammation and tissue injury, which occasionally causes dysplasia [8]. IBD have been associated with abnormal intestinal epithelial barrier function [9,10]. However, the underlying molecular mechanisms of IBD remain largely ambiguous.

Intestinal inflammation is usually accompanied by excessive production of reactive oxygen. High levels of reactive oxygen species (ROS) create oxidative stress within the cells and lead to a loss of homeostasis [11]. Redox imbalance has been proposed as one potential cause factor for IBD [12]. Oxidative stress plays an important role in the development and progression of IBD, and is associated with CRC pathogenesis [13–15]. In the gastrointestinal tract, oxidative stress leads to damage of the intestinal mucosal layer and epithelial cell apoptosis, which results in bacterial invasion in the gut and in turn stimulates the immune

* Corresponding author. Stem Cell Research Center, Ren Ji Hospital, School of Biomedical Engineering & Med-X Research Institute, Shanghai Jiao Tong University, 160 Pujian Road, Shanghai, 200127, China.
** Corresponding author. Stem Cell Research Center, Ren Ji Hospital, School of Biomedical Engineering & Med-X Research Institute, Shanghai Jiao Tong University, 160 Pujian Road, Shanghai, 200127, China.
E-mail addresses: gao.weiqiang@sjtu.edu.cn (W.-Q. Gao), lil@sjtu.edu.cn (L. Li).

https://doi.org/10.1016/j.redox.2021.102004
Received 21 December 2020; Received in revised form 19 April 2021; Accepted 7 May 2021
Available online 13 May 2021

response [16–18]. Clinical studies show that the increase of ROS and biomarkers of oxidative injury contributes to tissue damage in IBD [18,19]. Our previous work has also shown that excess ROS leads to defects in barrier integrity and the subsequent inflammation [20]. In order to resist the oxidative damage, the intestinal epithelium contains an extensive system of antioxidants [21,22]. Colitis is usually associated with a decrease in the levels of antioxidants in colonic tissues [19], whereas overexpression of antioxidant enzymes results in attenuation of colitis in mice [17]. Thus, a balance between oxidant and antioxidant mechanisms is necessary to maintain intestinal epithelial homeostasis.

Epigenetic regulation disorder is important in the onset and pathogenesis of IBD [23–25], which may influence the maintenance of homeostasis in the intestinal epithelium. Studies have shown that DNA methylation is correlated with disease susceptibility and progression in IBD [26,27]. It is also known that inactive histone modification H3K27 trimethylation regulated by EZH2 promotes the inflammatory response and apoptosis in colitis [28]. Moreover, our previous study has also shown that BRG1, a key epigenetic regulator, attenuates colonic inflammation and tumorigenesis through autophagy-dependent oxidative stress sequestration [20]. In addition, SETD2, a trimethyltransferase of histone H3 lysine 36 (H3K36), is frequently mutated (17%) in UC samples with a high risk of developing colorectal carcinoma [29], suggesting that SETD2 plays a potential role in colitis and colitis-associated CRC.

SETD2 is the only known H3K36 methyltransferase that can alter the trimethylation status of H3K36 and regulates protein structures as well as its function [30,31]. SETD2-induced H3K36me3 is a multifunctional histone marker associated with actively transcribed regions and is critical for many biological processes, such as transcriptional regulation, DNA damage repair, chromosome segregation and alternative splicing [32–35]. SETD2 has also been identified as a common mutation across cancer types, including glioma [36], renal cell carcinoma [34], leukemia [37,38] and lung cancer [39,40]. In addition, we have recently also reported that SETD2 is pivotal for bone marrow mesenchymal stem cells differentiation, genomic imprinting and embryonic development, initiation and metastasis of pancreatic cancer, and normal lymphocyte development [41–45]. However, functions of SETD2 in IBD and colitis -associated CRC remain largely undefined.

To investigate a possible role of SETD2 in IBD, in the present work we generated intestinal epithelium-specific *Setd2*-knockout mice, and found that deletion of *Setd2* in intestinal tissues promotes DSS-induced epithelial damage and subsequent tumorigenesis. Mechanistically, our results highlighted SETD2 as a critical epigenetic determinant in the prevention of colitis and tumorigenesis through modulation of oxidative stress.

2. Materials and methods

2.1. Mice

All mice were bred and maintained at an animal facility under specific pathogen-free conditions. *Setd2-flox* mice and *Villin-Cre* mice were purchased from Shanghai Biomodel Organism Co.. $Setd2^{Vil\text{-}KO}$ mice were generated by crossing *Setd2-flox* mice with *Villin-Cre* mice. All mice were maintained on C57BL/6 J background and littermates with the same treatment were used as controls in all experiments.

2.2. Human specimen analysis

Patients with IBD and non-IBD control subjects for this study were recruited from Renji hospital (Shanghai, China). The use of pathological specimens, as well as the review of all pertinent patient records, were approved by the Ethics Review Board of Renji hospital. Immunohistochemical analyses were performed using a specific anti-SETD2 antibody (LSBio, Cat# C332416). Protein expression was scored based on a multiplicative index of the average staining intensity (0–3) and the extent of staining (0–3), which yielded a 10-point staining index that ranged from 0 to 9.

2.3. Induction of colitis and CRC

To induce acute colitis, wild-type mice were fed with 3% dextran sodium sulfate (DSS; MP Biomedicals) for 7 days, which was then followed by 5 days of regular drinking water; $Setd2^{f/f}$ and $Setd2^{Vil\text{-}KO}$ mice were fed with 2% DSS for 5 days, which was then followed by 5 days of regular drinking water. For the N-acetyl-L-cysteine (NAC) (Sigma, A7250) treatment experiments, 8-week-old mice were pretreated with NAC (100 mg/kg) every day for 4 days induced by intraperitoneal injection, and treatment was continued during DSS administration for 5 days.

In AOM/DSS experiments, mice were treated with a single dose of AOM (10 mg/kg, Sigma), and 2% DSS was given in the drinking water for 5 days, followed by two weeks of regular drinking water. The DSS treatment was repeated for two additional cycles, and mice were sacrificed 90 days after AOM injection.

2.4. Isolation of intestinal epithelial cells and culture

For RNA-Seq and ChIP-Seq analyses, IECs were isolated as follows: mice were sacrificed and colonic specimens were dissected, opened longitudinally and cleared from feces by washing extensively in cold PBS. Colons were cut in small pieces of 1 mm and incubated in 30 mM EDTA solution in PBS at 37 °C for 10 min. 10 min later, EDTA solution was replaced with ice-cold PBS and shacked vigorously for 30 s. This process was repeated once more. Supernatants were collected and combined from both incubations, then centrifuged at 1200 rpm for 5 min at 4 °C. For culture purpose, the colons were cut into pieces and washed by DMEM for three times, and then incubated with digestion buffer containing 250 μg/ml collagenase type I (Sigma, C0130) and 500 μg/ml Dispase II (Roche #04942078001) for 1.5 h in 37 °C. After the incubation, the cell suspension was passed through 100 μm cell strainers (Corning). After washes, the cells were plated in dishes coated with rat tail tendon collagen type I overnight and were cultured in DMEM with 10% FBS and 1% penicillin/streptomycin. The purities of colonic epithelial cell from the EDTA-based and enzymatic digests were 90–95% and 80–85%, respectively, using an EpCAM antibody (Invitrogen #25-5791-80) and FACS analysis.

2.5. Isolation of lamina propria cells and flow cytometry analysis

Colons were cut into small pieces and incubated in 5 mM EDTA solution in PBS at 37 °C for 30 min with gentle shaking. After removal of the epithelial layer, the remaining colon pieces were incubated at 37 °C with RPMI medium containing 1.75 mg/ml collagenase A (Roche #10103586001) and 0.05 mg/ml DNase I (Roche #104159) for 45 min. After digestion, the supernatant was passed through a 70 μm cell strainer to isolate lamina propria cells. Lamina propria cells were stained for surface markers CD4, CD11b, F4/80 and Gr-1, and subjected to flow cytometry analyses. The antibodies used are listed in Supplementary Table 2.

2.6. Organoid culture and analysis

The intestines were opened longitudinally, and villi were scraped away. The pieces were thorough washed in cold PBS, and incubated in 2 mM EDTA solution in PBS for 10 min at 4 °C. Then, EDTA solution was replaced with PBS and shacked vigorously for 45 s. Crypt fractions were purified by successive centrifugation steps. For every 500-1,000 crypts, a mixture of 100 μL Matrigel (BD Biosciences) and complete growth medium (ratio 2: 1) is added. After polymerization, 100 μl Advanced DMEM/F12 (Invitrogen) containing EGF (50 ng/ml, PeproTech), R-spondin (500 ng/ml, PeproTech), Noggin (100 ng/ml, PeproTech), N-

acetyl-1-cysteine (1 μM, Sigma-Aldrich), N2 (1X, Life Technologies) and B27 (1X, Life Technologies) was added and refreshed every two or three days. On the fifth day, the organoids were stained with 7-AAD (Invitrogen, A1310) for 5 min to detect apoptosis levels, and photos were imaged by Zeiss fluorescence microscope and quantified by Image J software. (The NAC concentration in organoid culture is extremely low (1 μM), which will not affect the level of ROS.)

2.7. RNA-seq assay and data analysis

IECs were isolated from $Setd2^{f/f}$ and $Setd2^{Vil-KO}$ mice treated for 4 d with DSS by EDTA-based isolation. Each sample contained 3 independent repeated animals. NEB Next Ultra Directional RNA Library Prep Kit for Illumina (New England Biolabs, Ipswich, MA, USA) was used for the construction of sequencing libraries. The libraries were then subjected to Illumina sequencing with paired-ends 2 × 150 as the sequencing mode. The clean reads were mapped to the mouse genome (assembly GRCm38) using the HISAT2 software. Gene expression levels were estimated using FPKM (fragments per kilobase of exon per million fragments mapped) by StringTie. Gene annotation file was retrieved from Ensembl genome browser 90 databases (http://www.ensembl.org/index.html). The false discovery rate (FDR) control method was used to calculate the adjusted P-values in multiple testing in order to evaluate the significance of the differences. The statistical significance of differentially expressed genes was analyzed using a p-value threshold of <0.05 and fold change ≥ 1.25. We obtained 18168 differentially expressed genes (644 genes were up-regulated, and 605 genes were down-regulated). All differentially expressed mRNAs were selected for gene ontology (GO) analysis. We downloaded the GO annotations from NCBI (http://www.ncbi.nlm.nih.gov/), UniProt (http://www.uniprot.org/) and the Gene Ontology (http://www.geneontology.org/). Fisher's exact test was applied to identify the significant GO categories (P-value < 0.05).

2.8. ChIP-seq assay and data analysis

IECs were isolated from $Setd2^{f/f}$ and $Setd2^{Vil-KO}$ mice after 4 d of DSS treatment. The fragmented chromatin fragments were pre-cleared and then immunoprecipitated with Protein A + G Magnetic beads coupled with anti-H3K36me3 (Abcam, ab9050, 2–3μg/1 × 10^6 cells) antibody and IgG antibody (CST, 2729S, 2–3μg/1 × 10^6 cells). After reverse crosslinking, ChIP and input DNA fragments were end-repaired and A-tailed using the NEBNext End Repair/dA-Tailing Module (E7442, NEB) followed by adaptor ligation with the NEBNext Ultra Ligation Module (E7445, NEB). The DNA libraries were amplified for 15 cycles and sequenced using Illumina NextSeq 500 with single-end 1 × 75 as the sequencing mode. Raw reads were filtered to obtain high-quality clean reads by removing sequencing adapters, short reads (length<50 bp) and low-quality reads using Cutadapt (v1.9.1) and Trimmomatic (v0.35). Then FastQC is used to ensure high reads quality. The clean reads were mapped to the mouse genome (assembly GRCm38) using the Bowtie2 (v2.2.6) software. Peak detection was performed using the MACS (v2.1.1) peak finding algorithm with 0.01 set as the p-value cutoff. In total, 178919 and 217927 H3K36me3 peaks were identified in $Setd2^{Vil-KO}$ and $Setd2^{f/f}$ IECs over the input control, respectively. The heat maps and average profile for TSS were generated using ngsplot v2.61.

2.9. Statistics

Data were analyzed using the student's t-test and results are presented as the mean + s.e.m (SEM) unless otherwise indicated. Pearson correlation coefficients were used to evaluate the relationships between SETD2 and gene expressions, and the Wilcoxon signed rank test was used for patient analysis. Statistical analysis was performed using the GraphPad Prism software. A p value that was less than 0.05 was considered statistically significant for all data sets.

For RNA isolation, Real-time PCR, Western blotting, Immunohistochemistry, Analysis of intestinal permeability, ROS detection, ChIP-qPCR, Plasmid construction, 16S-rDNA sequencing, antibiotics treatment and histopathological analysis, can be found in Supplementary methods. All the antibodies used are listed in Supplementary Table 2.

3. Results

3.1. SETD2 expression becomes decreased in IBD patients and DSS treated mice

To explore a possible role of SETD2 in IBD, we analyzed SETD2 mRNA expression in public datasets of IBD samples (using datasets from NCBI's Gene Expression Omnibus: GSE9452 and GSE3365). The results indicated that the level of SETD2 mRNA was reduced in IBD specimens compared with that in healthy controls (Fig. 1A). To validate these data in IBD, we performed quantitative RT-PCR (RT-qPCR) assays and immunohistochemistry analyses to determine SETD2 expression in colonic biopsy specimens from IBD patients as well as from normal controls. Compared with the levels in biopsies from healthy specimens, we showed that SETD2 mRNA levels were significantly decreased in the IBD patients (Fig. 1B). The quantification of the immunohistochemical results revealed that the protein levels of SETD2 in the colonic epithelial cells were significantly lower in the IBD specimens relative to that in the healthy subjects (Fig. 1C).

To further evaluate the relevance of SETD2 in IBD, we measured SETD2 expression level in a DSS-induced colitic mouse model (Supplementary Fig. 1A), which is a common mouse model that imitates the clinical pathology of IBD [46,47]. The DSS-treated wild-type mice exhibited epithelial erosions and inflammation in the colon (Fig. 1D). Consistently, the DSS-treated colons produced significantly more proinflammatory cytokines and chemokines than the colons from control littermates (Supplementary Fig. 1B). These results indicated that we successfully established a colitic mouse model. To identify cellular populations expressing SETD2 in the colon, we performed co-immunofluorescence staining of SETD2 with E-cadherin, ChgA (Enteroendocrine cells), DCLK1 (Tuft cells), F4/80 and CD4, respectively, in the colon of wild-type mice. $SETD2^+$ cells were located along the intestinal epithelium and SETD2 was co-expressed with E-cadherin, ChgA, DCLK1, F4/80 and CD4 respectively (Supplementary Fig. 1C), indicating that SETD2 is expressed in both epithelial cells and non-epithelial cells in the colon. Subsequently, we evaluated SETD2 expression in the intestine of colitic mice. Similar to what was seen in IBD patients, SETD2 was down-regulated in the intestine of DSS-induced colitic mice (Fig. 1E–G). Together, these findings suggest a potential link between SETD2 reduction and IBD pathogenesis.

3.2. $Setd2^{Vil-KO}$ mice are more susceptible to DSS-induced colitis

To assess a role of SETD2 in colonic inflammation, we crossed *Setd2-flox* mice ($Setd2^{f/f}$ mice) with *Villin-Cre* mice to obtain an intestinal epithelium-specific *Setd2* knockout mouse strain (*Villin-Cre*; *Setd2 flox/flox* mice, hereinafter referred to as $Setd2^{Vil-KO}$ mice). As expected, *Setd2* was efficiently ablated and H3K36me3 was substantially reduced in the intestinal epithelium of $Setd2^{Vil-KO}$ mice by immunohistochemical staining and immunoblot validation (Fig. 2A–B). Histological examination of 8-week-old $Setd2^{Vil-KO}$ mice revealed no obvious abnormalities in the colon crypt (Supplementary Fig. 2A). However, as compared to the $Setd2^{f/f}$ mice, the levels of several proinflammatory cytokines and chemokines (IL-1α, CXCL1) were significantly higher in the colonic sections of $Setd2^{Vil-KO}$ mice (Supplementary Fig. 2B and 2C). Meanwhile, $Setd2^{Vil-KO}$ mice exhibited abnormal decreases of mucus-producing goblet cells and AMP-producing Paneth cells (Supplementary Fig. 2D). The two types of cells play important roles in intestinal antibacterial defense by releasing antimicrobial factors [48,49]. These observations were further confirmed by RT-qPCR analysis (Supplementary Fig. 2E).

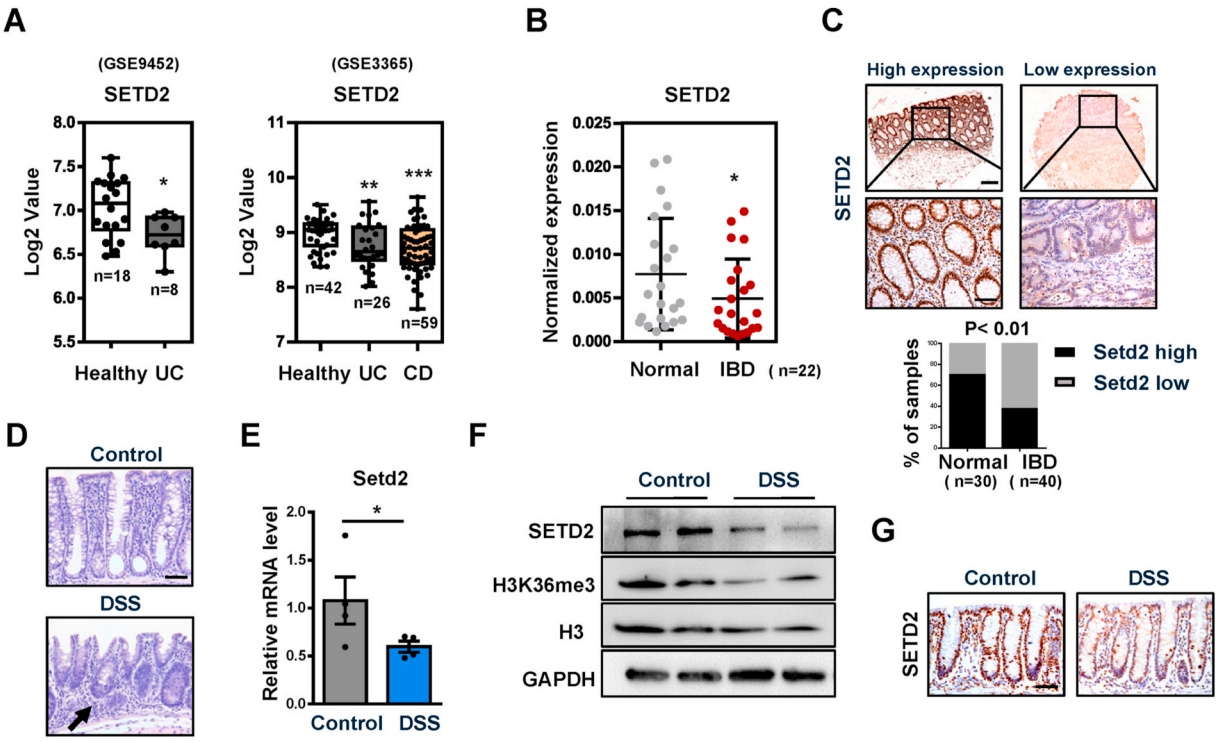

Fig. 1. SETD2 expression is downregulated in IBD patients and DSS treated mice.
(A) Boxplot of SETD2 expression levels in healthy controls and IBD specimens (using dataset GSE9452 and GSE3365).
(B) RT-qPCR analysis of SETD2 mRNA in IBD specimens and healthy subjects (n = 22 per group).
(C) SETD2 staining images are shown in the upper panel, and epithelial SETD2 expressions in normal and IBD biopsies are quantified in the bottom panel ($\chi 2$ test). Staining indexes use a 10-point quantification scale, and a score >4 is considered higher level. Scale bar: 100 μm (upper), 50 μm (bottom).
(D–G) Samples are all derived from 8-week-old wild-type mice with or without 3%DSS treatment (n = 4 per genotype).
(D) Representative images of H&E-stained colon sections as indicated. Arrow: immune cell infiltration. Scale Bars: 50 μm.
(E) RT-qPCR analysis of SETD2 mRNA in IECs from control and DSS-treated wild-type mice (n = 4 per genotype).
(F) Immunoblot analyses of SETD2 expression in IECs from control and DSS-treated wild-type mice are shown, and quantitation results are shown in the right.
(G) Immunohistochemical of SETD2 expression in control and DSS-treated wild-type mice are shown. Scale Bars: 50 μm.
The data represent the mean ± S.E.M, and statistical significance was determined by a two-tailed Student's *t*-test. *p < 0.05, **p < 0.01 and ***p < 0.001.

To further define the role of SETD2 in colitis, we assessed the consequence of *Setd2* loss in acute colitis by challenging $Setd2^{f/f}$ and $Setd2^{Vil\text{-}KO}$ mice with 3% DSS for 7 days and then monitored their susceptibility. We noticed that $Setd2^{Vil\text{-}KO}$ mice exhibited hypersusceptibility to 3% DSS-induced acute colitis, and most of the $Setd2^{Vil\text{-}KO}$ mice survived no longer than 10 days of observations. Therefore, the mice were switched to a lower dose of DSS (2%) and shorter treatment time (5 days) challenge (Fig. 2C) to induce acute colitis. After DSS administration, $Setd2^{Vil\text{-}KO}$ mice lost more body weight than $Setd2^{f/f}$ mice (Fig. 2D), suggesting that $Setd2^{Vil\text{-}KO}$ mice probably had enhanced inflammation and intestinal damage, as body weight loss is one of the characteristics for the severity of DSS-induced colitis [50,51]. In addition, macroscopic dissection revealed significantly shorter colons in the $Setd2^{Vil\text{-}KO}$ mice compared with the $Setd2^{f/f}$ mice (Fig. 2E). On further histopathological examination, the $Setd2^{Vil\text{-}KO}$ mice exhibited widespread damage in the colon, with more ulcerations as compared with $Setd2^{f/f}$ mice. At 10 days post DSS treatment, the $Setd2^{f/f}$ colon showed minimal to mild inflammation, while colon from $Setd2^{Vil\text{-}KO}$ mice displayed moderate to severe inflammation, with many areas of complete crypt loss and erosions (Fig. 2F). The excess inflammatory response observed in the $Setd2^{Vil\text{-}KO}$ mice was also associated with a loss of goblet cells and Paneth cells, and protein level of MUC2 secreted by goblet cells was also decreased in $Setd2^{Vil\text{-}KO}$ mice (Fig. 2G, Supplementary Fig. 2F). Since $Setd2^{Vil\text{-}KO}$ mice showed higher epithelial damage and inflammation, we then analyzed immune cell infiltration by performing flow cytometry. At 5 days post DSS treatment, we observed a higher number of CD4 + T cells, neutrophils, and macrophages in $Setd2^{Vil\text{-}KO}$ mice compared with control mice (Fig. 2H and Supplementary Fig. 2G). Notably, the immune cell infiltration also extended to the entire colon, as evidenced by the accumulation of F4/80-positive cells in relatively non-inflamed areas of the $Setd2^{Vil\text{-}KO}$ colons (Fig. 2I). It is well-known that infiltrating immune cells produce cytokines and chemokines to resolve the inflammation process [52,53]. As expected, the DSS-treated $Setd2^{Vil\text{-}KO}$ colons produced prominently more proinflammatory cytokines and chemokines than the colons from the $Setd2^{f/f}$ littermates (Fig. 2J and Supplementary Fig. 2H). Collectively, these results demonstrate that depletion of *Setd2* leads to exacerbated colitis, suggesting that SETD2 plays a pivotal role in attenuating inflammatory response in experimental colitis.

3.3. *Setd2* deficiency facilitates the formation of colitis-associated CRC

The observation that $Setd2^{Vil\text{-}KO}$ mice suffered from the sustained inflammation, prompted us to investigate a possible role of SETD2 in colitis-associated tumorigenesis. We induced CRC by injecting the DNA-methylating agent azoxymethane (AOM), followed by three cycles of 2% DSS treatments, and each cycle consisted of 5 days of 2%DSS water followed by 14 days of water alone. We recorded the changes in body weight throughout the duration of the AOM/DSS treatment, and determined the tumor burden 90 days after the AOM injection. We found that $Setd2^{Vil\text{-}KO}$ mice suffered from chronic inflammation and lost noticeably more body weight compared with the control mice (Fig. 3A). Compared with the $Setd2^{f/f}$ mice, *Setd2*-deficient mice had more macroscopic polypoid lesions, which were on average threefold larger in size

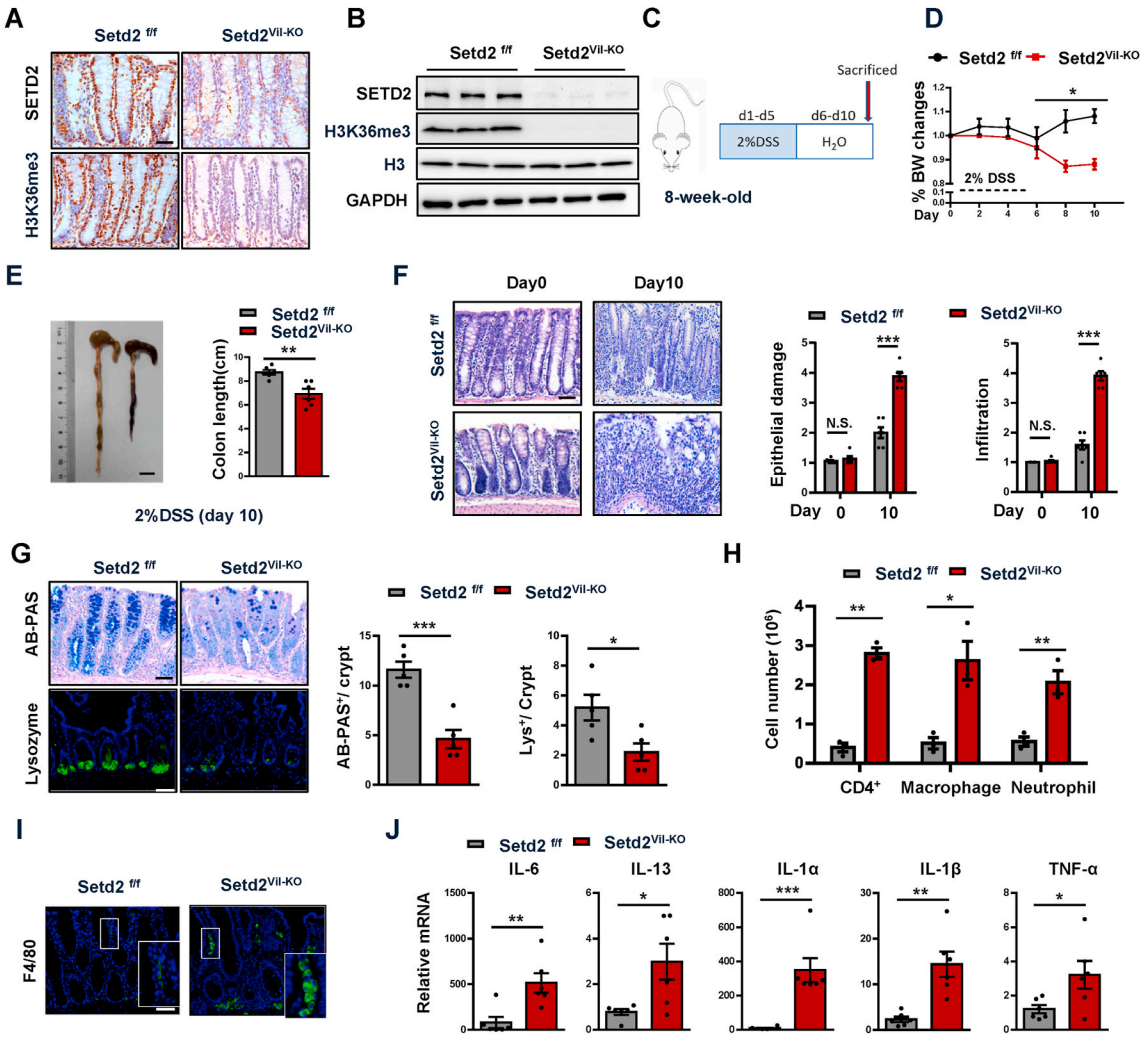

Fig. 2. Loss of *Setd2* in IECs aggravates DSS-induced colitis in mice.

(A) Immunohistochemical analyses of SETD2 and H3K36me3 expressions are shown.

(B) Immunoblot analyses of SETD2 and H3K36me3 expression in IECs from *Setd2*$^{Vil\text{-}KO}$ and *Setd2*$^{f/f}$ mice are shown. Scale Bars: 20 μm.

(C) Schematic representation of the DSS protocol used to induce acute colitis in *Setd2*$^{Vil\text{-}KO}$ and *Setd2*$^{f/f}$ mice.

(D, E) *Setd2*$^{Vil\text{-}KO}$ and *Setd2*$^{f/f}$ mice were fed 2% DSS in drinking water, and loss of body weights (D) and colon length (E) are recorded (n = 6 per genotype). Scale Bars: 1 cm.

(F) H&E stained sections of colon tissues collected on day 0 and 10 from 2% DSS-treated *Setd2*$^{Vil\text{-}KO}$ and *Setd2*$^{f/f}$ mice, and the quantitation of DSS-induced epithelial damage and immune cell infiltration are shown in the right (n = 6 per genotype). Scale Bars: 50 μm.

(G) Alcian blue-Periodic acid Schiff (AB-PAS; goblet cells) staining in the colon and lysozyme (Lys; Paneth cells) staining in the small intestine as indicated (n = 6 per genotype). Scale Bars: 20 μm.

(H) After 5 d of DSS treatment, colonic lamina propria cells from *Setd2*$^{Vil\text{-}KO}$ and *Setd2*$^{f/f}$mice are analyzed by flow cytometry for CD4 + T cells, CD11b +; F4/80 + macrophages, and CD11b +; Gr-1 + neutrophils (n = 3 per genotype).

(I) Colon sections from mice treated with DSS were stained for F4/80 to detect macrophages. Scale Bars: 50 μm.

(J) Relative mRNA expression levels of inflammatory mediators in whole colon of *Setd2*$^{Vil\text{-}KO}$ and *Setd2*$^{f/f}$ mice were determined by RT-qPCR (n = 6 per genotype). The data represent the mean ± S.E.M, and statistical significance was determined by a two-tailed Student's *t*-test. *p < 0.05, **p < 0.01 and ***p < 0.001. N.S., Not Significant. (For interpretation of the references to color in this figure legend, the reader is referred to the Web version of this article.)

(Fig. 3B). Histological analysis revealed that around 50% of polyps in *Setd2*$^{Vil\text{-}KO}$ mice were classified as high-grade dysplasia. However, the lesions developed in *Setd2*$^{f/f}$ mice were mainly graded as low-grade dysplasia or hyperplasia (Fig. 3C). Accordingly, the colons of *Setd2*$^{Vil\text{-}KO}$ mice exhibited higher proliferative rates, indicated by Ki67 staining, than those in the control mice (Fig. 3D). Thus, *Setd2* ablation results in increased inflammatory response, which facilitates the development and progression of colitis-associated CRC.

3.4. Disruption of Setd2 induces intestinal epithelium apoptosis and barrier damage in experimental colitis

Given that intestinal epithelial barrier dysfunctions could frequently contribute to gut inflammation [7,9,10], and that there were increased epithelial damage in the absence of *Setd2* (Fig. 2F), we investigated whether the loss of *Setd2* compromised the barrier integrity by assessing the distribution of junction proteins and permeability of intestinal colonic mucosa. We examined the distribution of the tight junction protein 1 (ZO-1), E-cadherin, Claudin-1 and Claudin-2 in *Setd2*$^{f/f}$ and *Setd2*$^{Vil\text{-}KO}$ mice, four markers to reveal the intercellular junctions of intestinal colonic mucosa. In contrast to the controls, the *Setd2*-deficient

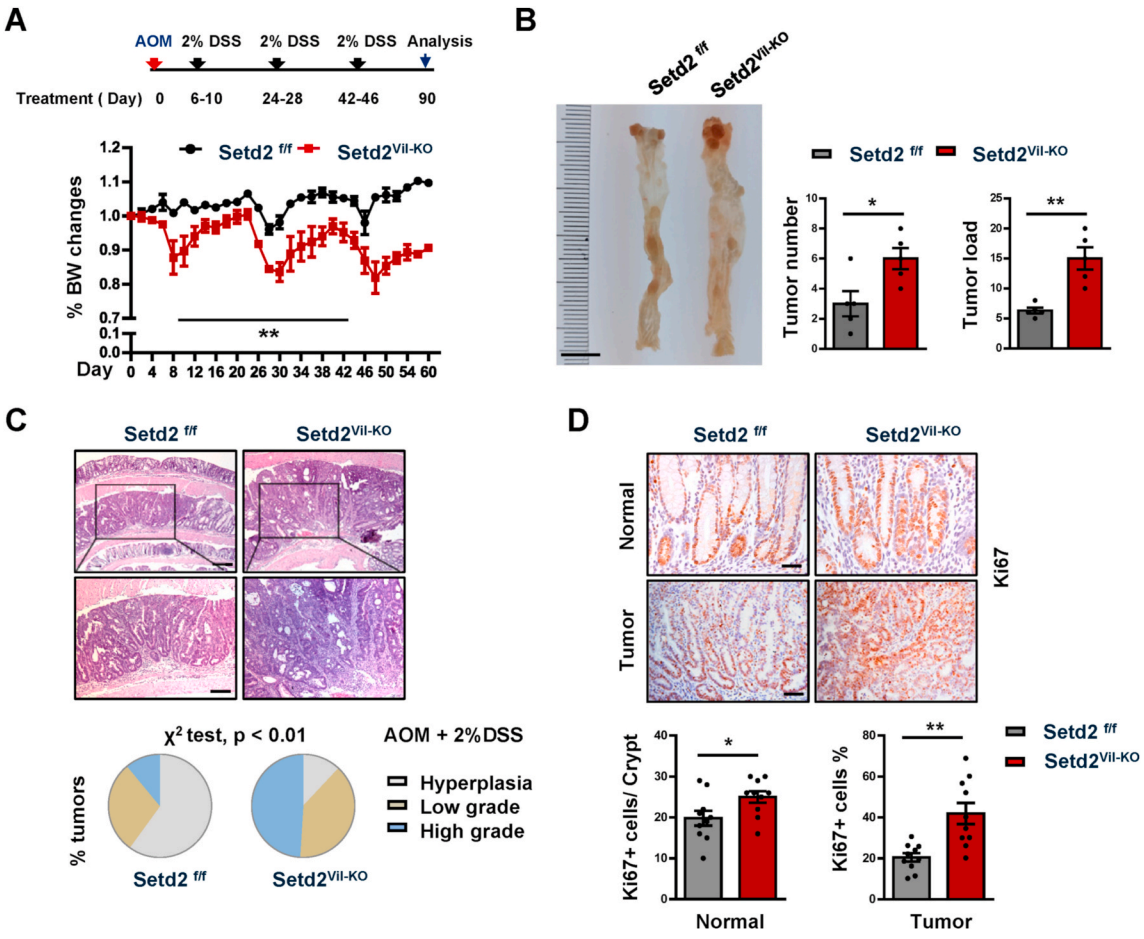

Fig. 3. ***Setd2*** **loss promotes the colitis -associated CRC.**
(A) *Setd2*$^{Vil\text{-}KO}$ and *Setd2*$^{f/f}$ mice were injected with AOM on day 0 (2 months of age) and treated with 2% DSS during three 5-day cycles as indicated. Body weight changes are recorded as indicated (n = 5 per genotype).
(B) At day 90 after the AOM injection, the mice were sacrificed to examine the tumor burden (n = 5 per genotype). Scale Bars: 1 cm.
(C) Representative images of colons and the overall grading of the tumors in each genotype (χ2 test) are shown (n = 5 per genotype). Scale Bars: 200 μm (upper), 100 μm (bottom).
(D) Representative images of Ki67 staining in normal colons and tumors from AOM/DSS-treated *Setd2*$^{Vil\text{-}KO}$ and *Setd2*$^{f/f}$ mice are shown (n = 5 per genotype). Scale Bars: 20 μm (upper), 50 μm (bottom). The data represent the mean ± S.E.M, and statistical significance was determined by a two-tailed Student's *t*-test. *p < 0.05, **p < 0.01.

colons showed partially disrupted or discontinuous ZO-1, E-cadherin, Claudin-1 and Claudin-2 staining (Fig. 4A, Supplementary Fig. 3A), indicating that an intact mucosal barrier was compromised in *Setd2*$^{Vil\text{-}KO}$ mice. This observation was further strengthened by Western blot and RT-qPCR analyses showing reduced expression of ZO-1, E-cadherin, Claudin-1 and Claudin-2 in *Setd2*$^{Vil\text{-}KO}$ mice compared with control mice (Fig. 4B, Supplementary Fig. 3B). In accordance with the severe ulceration (Fig. 2F), intestinal permeability was markedly increased in *Setd2*$^{Vil\text{-}KO}$ mice, evidenced by the enhanced fluorescence in the serum of DSS-treated *Setd2*$^{Vil\text{-}KO}$ mice fed with FITC-labeled dextran (Fig. 4C). Thus, these results indicate that *Setd2* deletion in colons leads to epithelial barrier damage and colonic leakage in experimental colitis.

Considering that epithelial apoptosis is one of the mechanisms by which DSS can induce intestinal inflammation or colitis, and that the epithelial barrier is disrupted in the absence of *Setd2* (Fig. 4C), we examined possible defects in epithelial cell survival in the *Setd2*$^{Vil\text{-}KO}$ mice. On the histopathological examination, the numbers of TUNEL- and cleaved caspase-3-positive cells were significantly higher in the colon sections from the *Setd2*$^{Vil\text{-}KO}$ mice than in those from the *Setd2*$^{f/f}$ mice (Fig. 4D). This observation was further strengthened by western blotting showing markedly elevated signaling intensities of cleaved caspase-3 in *Setd2*$^{Vil\text{-}KO}$ mice compared with *Setd2*$^{f/f}$ mice (Fig. 4E). Besides, the expression of Annexin A1, α-tubulins and F-actin, which is related to epithelial restitution, was reduced in *Setd2*$^{Vil\text{-}KO}$ mice, suggesting that there is impairment in epithelial restitution in IECs lacking Setd2 (Supplementary Fig. 3C and 3D). We next established intestinal organoid cultures to assess whether loss of *Setd2* induces apoptosis in a cell-intrinsic manner. As shown by 7-aminoactinomycin D (7-AAD) whole-mount staining and cleaved caspase-3 immunostaining, the organoids lacking SETD2 displayed a substantial increase in apoptosis relative to the controls (Fig. 4F). Besides, the expression of ZO-1, E-cadherin, Claudin-1 and Claudin-2 was decreased in organoids lacking SETD2 (Supplementary Fig. 3E–3G). These data emphasize that SETD2 is required for the survival of IECs, whose defects might cause the barrier disruption and the subsequent inflammation.

3.5. SETD2 modulates ROS homeostasis to regulate colon inflammation

To further investigate the molecular mechanisms in which SETD2 regulates intestinal epithelial homeostasis, we performed RNA-seq analysis. Next-generation sequencing using RNA from *Setd2*$^{Vil\text{-}KO}$ and *Setd2*$^{f/f}$ IECs after 4 d of DSS treatment respectively revealed that the global transcriptome was changed dramatically in *Setd2*$^{Vil\text{-}KO}$ IECs compared to the *Setd2*$^{f/f}$ IECs, indicating a significant function of SETD2

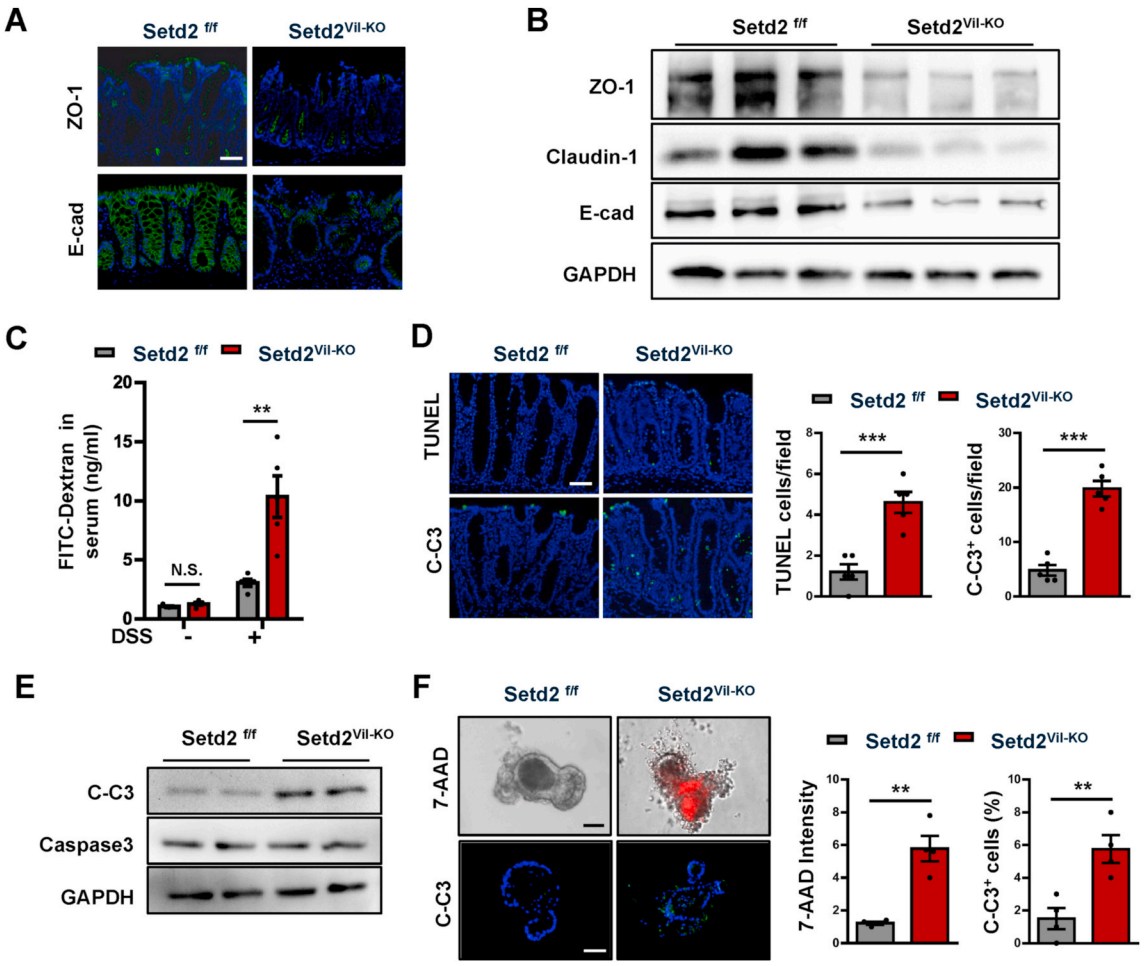

Fig. 4. Loss of *Setd2* in IECs induces cell apoptosis and barrier damage.

(A) Representative ZO-1 and E-cadherin staining in colon sections from DSS-treated (5 d) $Setd2^{Vil\text{-}KO}$ and $Setd2^{f/f}$ mice. Scale Bars: 100 μm.

(B) Immunoblotting analysis of the indicated proteins in IECs isolated from DSS-treated (5 d) $Setd2^{Vil\text{-}KO}$ and $Setd2^{f/f}$ mice.

(C) Colonic permeability was measured by the concentration of FITC-dextran in the blood serum (n = 5 per genotype).

(D) TUNEL (Upper) and cleaved caspase 3 (Lower) staining of colon sections from DSS-treated (5 d) $Setd2^{Vil\text{-}KO}$ and $Setd2^{f/f}$ mice, and quantitation results are shown in the right (n = 5 per genotype). Scale Bars: 50 μm.

(E) Western blot analysis of the indicated proteins in IECs isolated from DSS treated (5 d) $Setd2^{Vil\text{-}KO}$ and $Setd2^{f/f}$ mice.

(F) Intestinal organoids derived from $Setd2^{Vil\text{-}KO}$ and $Setd2^{f/f}$ mice. After 5 d of differentiation, 7-AAD-stained organoids (red) were imaged after 48 h (Upper), and quantitations of the fluorescence density are shown in the right. C-Casp3 staining of the organoid sections as indicated (Lower), and quantitation results are shown in the right (n = 4 per genotype). Scale Bars: 20 μm.

The data represent the mean ± S.E.M, and statistical significance was determined by a two-tailed Student's *t*-test. $^{**}p < 0.01$, $^{***}p < 0.001$. N.S., Not Significant. (For interpretation of the references to color in this figure legend, the reader is referred to the Web version of this article.)

in IECs (Fig. 5A). Among a total of 18168 genes expressed, 644 genes were up-regulated, and 605 genes were down-regulated (Fold change > 1.25) in $Setd2^{Vil\text{-}KO}$ IECs. Gene Ontology (GO) term analysis indicated that there was a significant enrichment of genes linked to apoptotic regulation and inflammatory response (Fig. 5A), which is consistent with previous observation (Figs. 2J and 4D). Interestingly, some genes related to "cellular response to oxygen levels" and "oxidation-reduction process" were also significantly enriched (Fig. 5A). These results were validated by RT-qPCR (Supplementary Fig. 4A). Of note, the mRNA expression levels of some antioxidant genes were significantly down-regulated, suggesting increased oxidative stress in the absence of *Setd2*. To confirm this finding, we performed 8-oxo-2′-deoxyguanosine (8-OHdG) staining to examine oxidative stress in colon. We detected that 8-OHdG level was significantly increased in the colon and organoid of $Setd2^{Vil\text{-}KO}$ mice after DSS treatment (Fig. 5B, Supplementary Fig. 4B). Oxidative stress is associated with intestinal inflammation and CRC pathogenesis, and ROS plays an important role in apoptosis induction and inflammatory damage under both physiologic and pathologic conditions [13,14]. Therefore, we studied the role of ROS in SETD2-mediated inflammation by staining using 2′,7′-dichlorodihydrofluorescein diacetate (H2DCFDA), which is a fluorescent probe that reacts with ROS. IECs were isolated from $Setd2^{Vil\text{-}KO}$ and $Setd2^{f/f}$ mice after DSS treatment, and flow cytometry analysis indicated that *Setd2*-deficency IECs produced significantly more amount of ROS relative to that in the control IEC cells (Fig. 5C).

To provide evidence that ROS indeed contributes to the barrier defects and colitis, we performed rescue assays to determine whether blocking ROS could reverse the inflammatory phenotype caused by the *Setd2* loss. Two-month-old $Setd2^{Vil\text{-}KO}$ and $Setd2^{f/f}$ mice were pretreated with an antioxidant, N-acetyl-L-cysteine (NAC) every day for 4 days, and treatment was continued during DSS administration for 5 days [13,54]. According to colon length and histopathological staining (Fig. 5D–E), the blockade of ROS production via the administration of NAC in the $Setd2^{Vil\text{-}KO}$ mice greatly eased the severity of inflammation, and the colonic morphology score was restored to the normal value. 8-OHdG level was significantly decreased in the colon of $Setd2^{Vil\text{-}KO}$ mice after

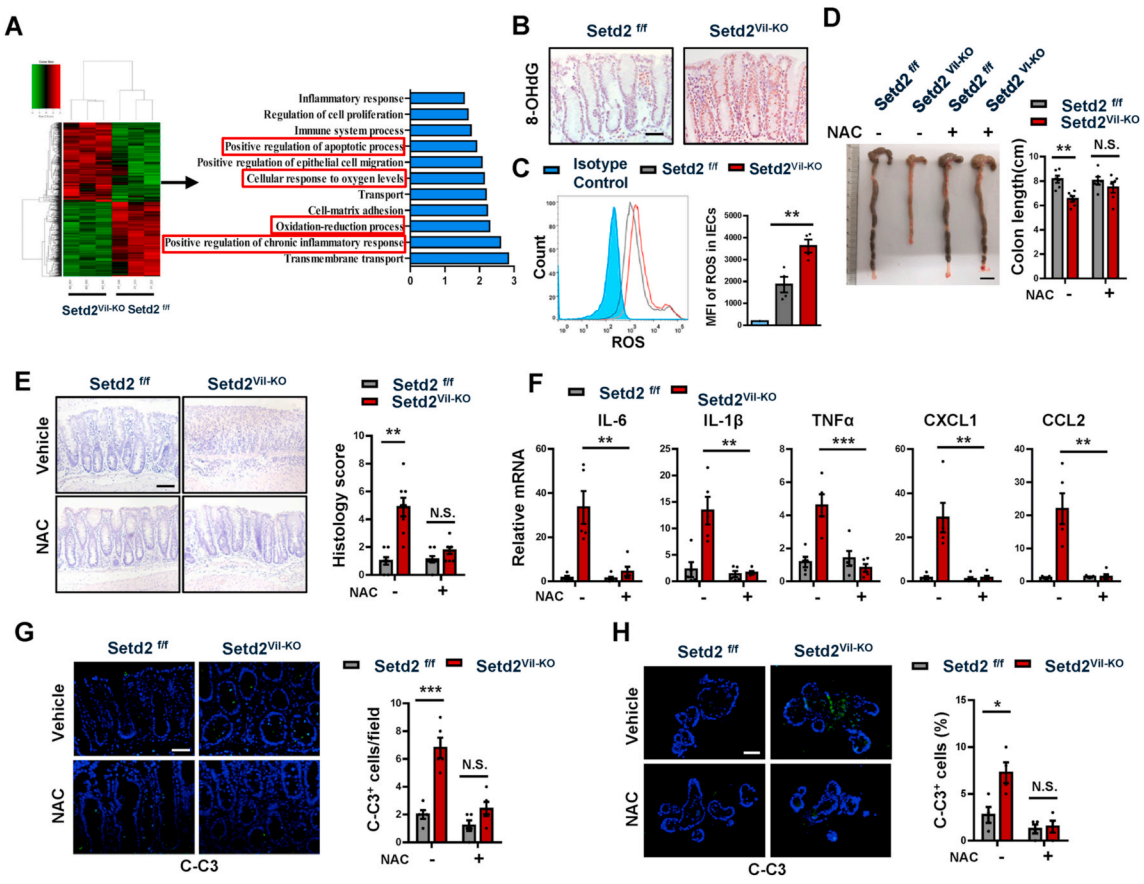

Fig. 5. SETD2 mediates ROS reaction to control cell apoptosis and colon inflammation.

(A) Heat map of RNA-seq data to compare the gene expression in the IECs from *Setd2*$^{Vil\text{-}KO}$ and *Setd2*$^{f/f}$ mice treated for 4 d with DSS. Go term analysis of gene expression changes in the right.

(B) 8-OHdG staining from DSS-treated (5d) *Setd2*$^{Vil\text{-}KO}$ and *Setd2*$^{f/f}$ mice. Scale Bars: 50 μm.

(C) Histograms and MFI quantifications of ROS in IECs isolated from DSS-treated (5d) *Setd2*$^{Vil\text{-}KO}$ and *Setd2*$^{f/f}$ mice (n = 4 per genotype).

(D–H) 8-week-old *Setd2*$^{Vil\text{-}KO}$ and *Setd2*$^{f/f}$ mice were pretreated with NAC (100 mg/kg) every day for 4 days induced by intraperitoneal injection, and treatment was continued during DSS administration for 5 days.

(D) The mice were euthanized on days 10 to measure colon length (n = 6 per genotype). Scale Bars: 1 cm.

(E) H&E stained sections of colon tissues collected on day 10 from DSS-treated mice as indicated, and semi-quantitative scoring of the histopathology is shown in the right (n = 6 per genotype). Scale Bars: 100 μm.

(F) Relative mRNA expression levels of inflammatory mediators in whole colon from DSS-treated (5 d) mice as indicated (n = 5 per genotype).

(G) Cleaved caspase-3 staining of colon sections from DSS-treated (5 d) *Setd2*$^{Vil\text{-}KO}$ and *Setd2*$^{f/f}$ mice with or without NAC treatment (n = 5 per genotype). Scale Bars: 50 μm.

(H) Organoids were isolated from 8-week-old *Setd2*$^{Vil\text{-}KO}$ and *Setd2*$^{f/f}$ mice with or without NAC treatment, and cleaved caspase-3 staining (n = 4 per genotype). Scale Bars: 20 μm.

The data represent the mean ± S.E.M, and statistical significance was determined by a two-tailed Student's *t*-test. *p < 0.05, **p < 0.01, ***p < 0.001. N.S., Not Significant. MFI, Median Fluorescence Intensity.

NAC treatment (Supplementary Fig. 4C). As judged by the expression levels of proinflammatory cytokines and chemokines, the severe inflammatory response occurring in the *Setd2*$^{Vil\text{-}KO}$ mice was largely mitigated by the ROS inhibition (Fig. 5F). Additionally, the NAC treatment restored the numbers of Paneth and goblet cells to levels similar to those in the control mice (Supplementary Fig. 4D and 4E). Besides, NAC-treated *Setd2*$^{Vil\text{-}KO}$ mice exhibited a less intestinal permeability, barrier disruption and epithelial cell apoptosis than *Setd2*$^{f/f}$ mice (Supplementary Fig. 4F–4H and Fig. 5G). In addition, the relieved 8-OHdG level, barrier defects and epithelial apoptosis were also repeated in intestinal organoid culture experiment (Supplementary Fig. 4I-4L and Fig. 5H). These results suggest that the blockade of ROS could reverse the phenotype of epithelial barrier disruption and colon inflammation in *Setd2*$^{Vil\text{-}KO}$ mice. Altogether, ROS plays an important role in experimental colitis exacerbated by SETD2 deficiency.

3.6. SETD2-mediated H3K36me3 facilitates the transcriptions of antioxidant genes to maintain ROS homeostasis

To elucidate the molecular basis by which SETD2 modulated ROS, we immunoprecipitated H3K36me3-bound chromatin in *Setd2*$^{Vil\text{-}KO}$ and *Setd2*$^{f/f}$ IECs after 4 d of DSS treatment and analyzed the precipitated DNA by deep sequencing. 178919 and 217927 H3K36me3 peaks were identified in *Setd2*$^{Vil\text{-}KO}$ and *Setd2*$^{f/f}$ IECs, respectively. The altered density of H3K36me3 intervals (*Setd2*$^{Vil\text{-}KO}$ versus *Setd2*$^{f/f}$) were widely localized within whole genomic regions, including gene bodies, promoters, and intergenic zones (Fig. 6A–B), indicating that SETD2 is responsible for the H3K36 trimethylaiton on these regions. To correlate the chromatin binding with the transcriptional regulation, we integrated the ChIP-seq data with the expression profile. The Venn diagrams indicated that 906 genes (including downregulated and upregulated genes) showed direct H3K36me3 occupancies and expression changes upon the *Setd2* ablation (Fig. 6C). GO term analysis revealed that these

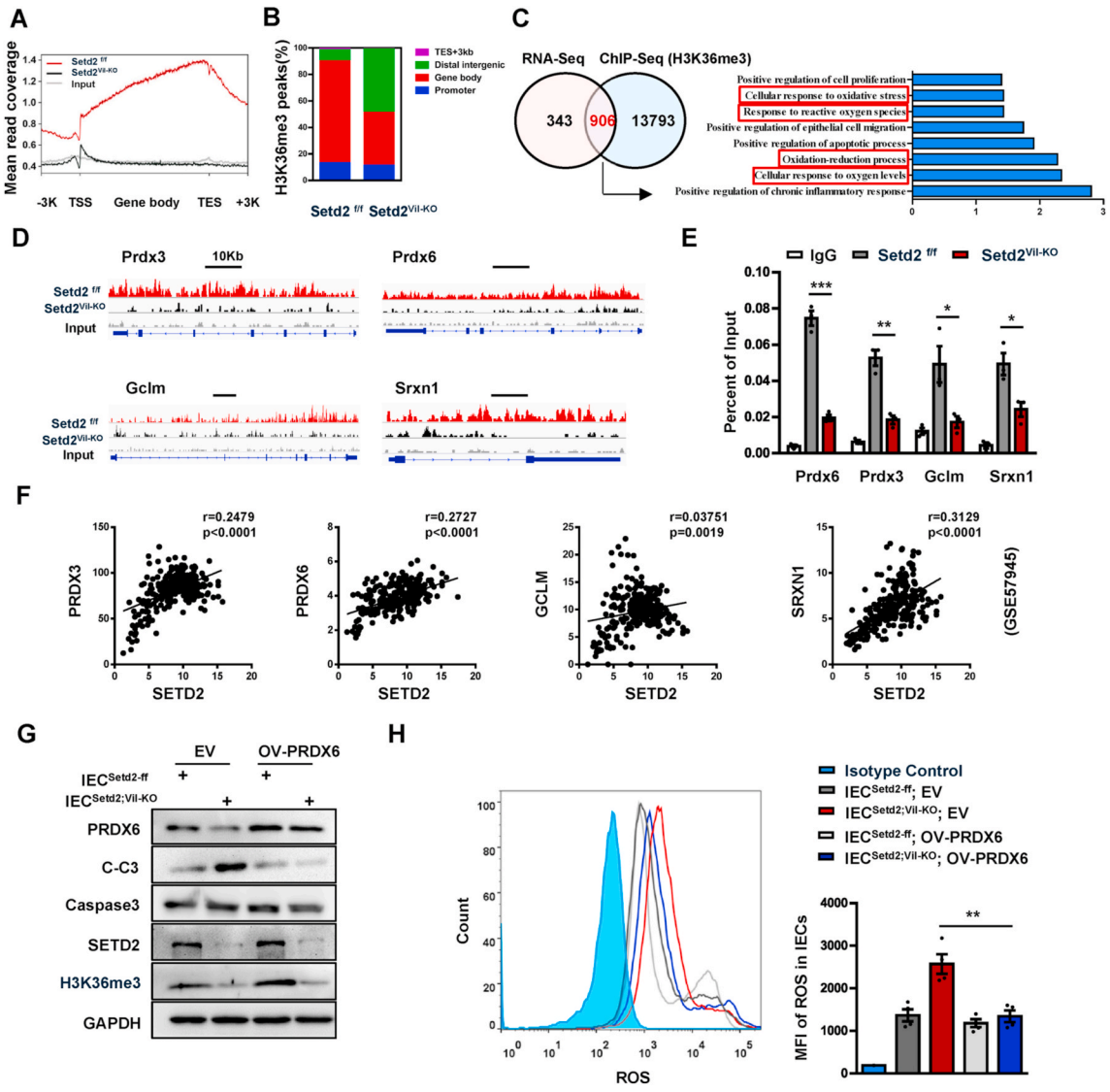

Fig. 6. SETD2 regulates antioxidant protein via H3K36me3.

(A) Normalized read density of H3K36me3 ChIP-seq signals in IECs isolated from *Setd2*$^{Vil\text{-}KO}$ and *Setd2*$^{f/f}$ mice treated for 4 d with DSS.

(B) Analysis of the occupancy of H3K36me3 ChIP-seq peaks in gene bodies and intergenic regions.

(C) Venn diagram showing the number of genes harboring H3K36me3 binding and displaying expression changes in *Setd2*$^{Vil\text{-}KO}$ IECs. Right panel shows the Go term analysis of the overlapping genes.

(D) Snapshot of H3K36me3 ChIP-Seq signals at the *Prdx3*, *Prdx6*, *Gclm* and *Srxn1* gene loci in IECs isolated from DSS-treated (4 d) *Setd2*$^{Vil\text{-}KO}$ and *Setd2*$^{f/f}$ mice.

(E) ChIP-qPCR analysis of H3K36me3 binding for *Prdx3*, *Prdx6*, *Gclm* and *Srxn1* loci in IECs from DSS-treated (4 d) *Setd2*$^{Vil\text{-}KO}$ and *Setd2*$^{f/f}$ mice, and IgG was used as the control (n = 3 per genotype).

(F) Correlation between SETD2 and PRDX3, PRDX6, GCLM and SRXN1 expression levels in IBD specimens (GSE 57945). Statistical significance was determined using the Pearson correlation coefficient.

(G) IECs were isolated from *Setd2*$^{f/f}$ and *Setd2*$^{Vil\text{-}KO}$ mice, and the corresponding are named as *IEC*$^{Setd2\text{-}ff}$ and *IEC*$^{Setd2;\ VIL\text{-}KO}$. Western blot analysis of the indicated proteins in*IEC*$^{Setd2\text{-}ff}$ and *IEC*$^{Setd2;\ VIL\text{-}KO}$ with or without PRDX6 overexpression.

(H) Histograms and MFI quantifications of ROS in *IEC*$^{Setd2\text{-}ff}$ and *IEC*$^{Setd2;\ VIL\text{-}KO}$ with or without PRDX6 overexpression (n = 4 per genotype).

The data represent the mean ± S.E.M, and statistical significance was determined by a two-tailed Student's *t*-test. *p < 0.05, **p < 0.01, ***p < 0.001. MFI, Median Fluorescence Intensity.

overlapping 906 genes were still closely related to oxidative stress pathway (Fig. 6C). As shown in Fig. 5, ablation of *Setd2* increased ROS production and down-regulated the expression levels of antioxidant genes, suggesting that Setd2/H3K36me3 might positively regulate some antioxidant-coding genes related to ROS production. As expected, antioxidant genes including *Prdx3*, *Prdx6*, *Gclm*, and *Srxn1* were listed among the 906 genes described above, and their downregulation was validated in colon epithelial cells collected from *Setd2*$^{Vil\text{-}KO}$ mice, comparing with cells from *Setd2*$^{f/f}$ mice (Supplementary Fig. 4A). Direct H3K36me3 occupancies within these candidate gene loci were also seen in Genome Browser tracks (Fig. 6D). We further validated the existence of H3K36me3 bindings at the gene bodies of *Prdx3*, *Prdx6*, *Gclm* and *Srxn1* by the ChIP-qPCR assays, and found that the intensity of H3K36me3 bindings within these gene loci decreased along with the loss of *Setd2* (Fig. 6E). Consistent with these results, there were significant positive correlations between mRNA levels of SETD2 and that of PRDX3, PRDX6, GCLM and SRXN1 respectively based on GSE57945 database (Fig. 6F). Thus, *Setd2* loss could repress the transcription of antioxidant genes, which were important for antioxidant defenses. The peroxiredoxin [PRDX] family contains the most of important antioxidant

proteins. PRDX6, a bifunctional 25-kDa protein, is one member of PRDXs [55]. Next, we sought to investigate whether restoration of PRDX6 in *Setd2*-depleted IECs would attenuate the overproduction of ROS and improve the cell survival as compared with *Setd2*-deleted IECs. As expected, overexpression of PRDX6 in *Setd2*-depleted IECs could significantly reduce the ROS production and the cleaved caspase-3 signals (Fig. 6G–H). Besides, PRDX6 overexpression could maintain the epithelial barrier and preserved cell junction proteins (Supplementary Fig. 5). Thus, ectopic *Prdx6* could alleviate the overproduction of ROS and improve the cellular survival in the *Setd2*-deficient intestinal epithelium. Together, these results indicate that SETD2 prevents colon inflammation and epithelial barrier defects via the regulation of antioxidant to maintain ROS homeostasis.

Gut microbes also play an important role in driving colonic inflammatory responses [6,56]. As compared with the $Setd2^{f/f}$ mice, there was less bacterial richness but unchanged gut microbiota composition in $Setd2^{Vil\text{-}KO}$ mice (Supplementary Fig. 6A and B). To rule out the possibility that the intestinal microbiota contributes to epithelial barrier damage caused by Setd2 deficiency, we generated gut microbiota-depleted mice by treating $Setd2^{Vil\text{-}KO}$ and $Setd2^{f/f}$ mice with drinking water containing an antibiotic cocktail for 4 weeks and then treated them with 2% DSS [57,58]. Interestingly, depletion of the gut microbiota by antibiotics eased the severity of colitis and reduced expression of proinflammatory cytokines and chemokines of $Setd2^{Vil\text{-}KO}$ mice comparable to those observed in the $Setd2^{f/f}$ mice (Supplementary Fig. 6C and D). However, antibiotic-treated $Setd2^{Vil\text{-}KO}$ mice still exhibited more severe barrier disruption, intestinal permeability, epithelial cell apoptosis and oxidative stress than $Setd2^{f/f}$ mice (Supplementary Fig. 6E-O). Moreover, the mRNA expression levels of some antioxidant genes (*Prdx3*, *Prdx6*, *Gclm*, and *Srxn1)* were still significantly down-regulated in antibiotic-treated $Setd2^{Vil\text{-}KO}$ mice compared with $Setd2^{f/f}$ mice (Supplementary Fig. 6P). These results suggested that depletion of the gut microbiota did not facilitate the recovery of intestinal barrier in $Setd2^{Vil\text{-}KO}$ mice. Thus, the gut microbiota does not contribute to intestinal barrier disruption caused by *Set*d2 deficiency. Considered together, SETD2 protects the colon epithelial barrier from inflammatory insults through a mechanism dependent on oxidative stress (Fig. 7).

4. Discussion

Although epigenetic dysregulation is recently believed to contribute to development of intestinal inflammation [25,26,59] and epithelial barrier disruption is one of the major causes of IBD, whether epigenetic elements are drivers during the regulation of epithelial barrier integrity and colonic inflammation and tumorigenesis has not been genetically determined. In this study, we established mice with epithelium-specific deletion of *Setd2* ($Setd2^{Vil\text{-}KO}$ mice), and then challenged with various inducing agents such as DSS and AOM to generate different types of models of colonic inflammation and tumorigenesis. We demonstrated clearly that deletion of *Setd2* that is responsible for one of the major histone modifications, disturbs intestinal epithelial homeostasis and worsens barrier defects by modulating oxidative stress, which promotes colonic inflammatory response and subsequent tumorigenesis (Fig. 7). Moreover, the excess inflammatory damage occurring in the *Setd2*-depleted mice was largely alleviated by the ROS inhibition through antioxidant NAC treatment. Our results highlight the importance that SETD2 functions as a homeostatic regulator that integrates the intact epithelial barrier by modulating oxidative stress in the colon. Support for our findings comes from a recent report indicating that mutations of the *Setd2* gene occur in up to 17% in UC samples with a high risk of developing colorectal carcinoma [29]. Thus, our study provides the first direct causal evidence that SETD2 plays a pivotal role in IBD and colitis-associated CRC.

The present study reveals a mechanism by which SETD2 inhibits ROS overreaction to maintain intestinal epithelial homeostasis against intestinal inflammation and tumorigenesis. ROS plays an important role in cell apoptosis induction and inflammation under both physiologic and pathologic conditions [13,14,20]. We found that *Setd2* deficiency in the colon epithelium leads to ROS accumulations, and then enhances epithelial cell death and barrier disruption. And this finding is further supported by the experiment of antioxidant NAC treatment. Therefore, excess ROS accumulation is mainly responsible for the colon inflammation observed in the $Setd2^{Vil\text{-}KO}$ mice. It is well known that SETD2 exerts epigenetic regulation via promoting the transcriptions of its downstream genes by marking gene bodies with H3K36me3 and facilitating the elongation of their pre-mRNA [60,61]. At molecular level, we show that *Setd2* deficiency down-regulates the mRNA levels of the members of antioxidant genes including *Prdx3*, *Prdx6*, *Gclm* and *Srxn1* in the analysis of sequencing results. The current findings demonstrate that SETD2 attenuates colonic inflammation through maintaining the expression of antioxidant genes to suppress oxidative stress. Clinically, we also found that expression level of SETD2 in IBD samples is positively correlated with the expressions of PRDX3, PRDX6, GCLM and SRXN1, respectively. *Setd2* deficiency led to epithelial barrier disruption accompanied by immune cell infiltration, such as CD4 + T cells, neutrophils, and macrophages (Fig. 2H), suggesting that immune cells might also play a role in the destruction of the epithelium. STAT signaling is

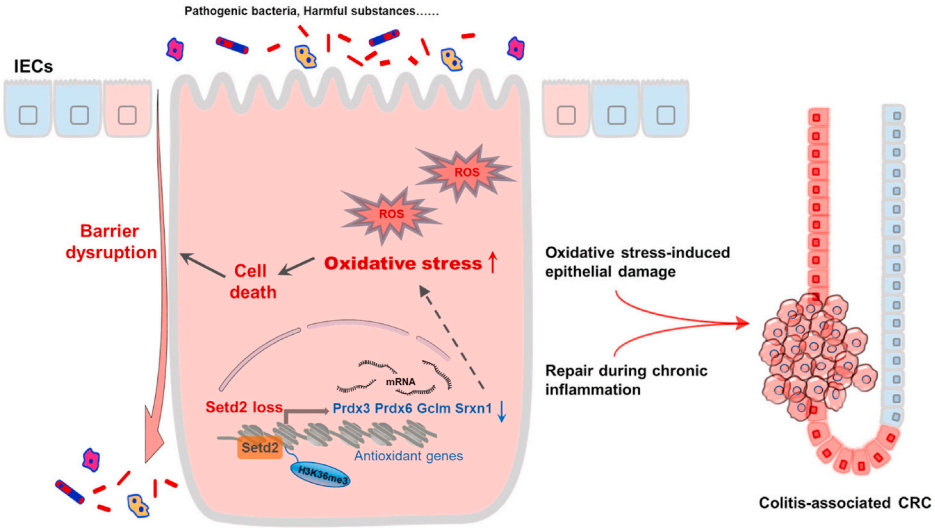

Fig. 7. Loss of *Setd2* promotes oxidative stress-induced colonic inflammation and tumorigenesis. SETD2 directly controls multifaceted antioxidant genes including *Prdx3*, *Prdx6*, *Gclm* and *Srxn1* in intestinal epithelial cells (IECs). Thus, *Setd2* loss in IECs leads to insufficient antioxidant, which results in excess reactive oxygen species (ROS), and thereby compromises barrier integrity and promotes inflammation. Compensatory regeneration coupled with oxidative stress-induced epithelial damage promotes the malignant progression of CRC.

involved in the proinflammatory response triggered in colitogenic macrophages and in colitic IEC [62,63]. In the present study, we also examined whether STAT signaling is altered in Setd2-depleted colons. There was no appreciable alternation of p-STAT1 expression level in the $Setd2^{Vil\text{-}KO}$ mice. However, p-STAT3 expression was increased in the $Setd2^{Vil\text{-}KO}$ mice, indicating activation of p-STAT3 (Supplementary Fig. 7). Therefore, our findings reveal for the first time the important role of SETD2-mediated H3K36me3 modification in the maintenance of intestinal epithelial homeostasis through the oxidative stress pathway, and provide insights into the molecular mechanisms underlying the intestinal inflammation and colitis-associated CRC with epigenetic disorders.

It is worth mentioning that SETD2 appears to interact with various proteins to influence transcription. Notably, our previous work reported that SETD2-mediated H3K36me3 could participate in cross-talks with other chromatin markers in oocytes, including H3K4me3 and H3K27me3 in transcribing regions [44]. In the present study, we demonstrate that expression of some antioxidant genes is regulated by SETD2-mediated H3K36me3. However, little is known about the epigenetic functions of other chromatin markers on regulating these genes in IBD. It would be interesting to study the physiological role of the cross-talk between H3K36me3 and other chromatin markers in IBD and colitis-associated CRC in the future. Moreover, recent studies have also revealed that SETD2 has the capacity to regulate cellular signaling through modification of non-histone substrates. For example, it has been reported that SETD2 could tri-methylate α-tubulin on K40 and mediate K525me1 of STAT1, which implicates a vital role in mitosis and antiviral immunity respectively [64,65]. In the present study, we show that SETD2-mediated H3K36me3 promotes the expression of some antioxidant genes. However, it remains to be determined whether SETD2 can interact with these proteins and methylate them to affect the progression of IBD and tumorigenesis.

5. Conclusions

Our findings highlight that SETD2 plays a critical role in the intestinal homeostasis and regulates barrier function and colon inflammation by modulating oxidative stress in the colon. We also established a SETD2/H3K36me3-deficient IBD mouse model that could be used for pre-clinical researches on colitis with epigenetic disorders. Given that SETD2 mutation accounts for 17% IBD patients with a high risk of developing colorectal carcinoma, our results may provide insight into our understanding of pharmaceutical investigation of these diseases associated with SETD2/H3K36me3 mutation.

Author contributions

M.L. mainly performed the experiments, analyzed the data and wrote the paper. H.R., X.L., J.L., W.F. and J.X. helped with the experiments. L. L. and W.Q.G. conceived the concept, designed the experiments and drafted the manuscript. All authors had edited and approved the final manuscript.

Data availability

All data are available from the authors upon reasonable request. RNA-Seq and ChIP-Seq raw data have been deposited in the Gene Expression Omnibus (GEO) under accession number GEO: GSE 151968.

Declaration of competing interest

The authors declare no competing interests.

Acknowledgements

This study was supported by funds from Ministry of Science and Technology of the People's Republic of China (2017YFA0102900 to W. Q.G.), National Natural Science Foundation of China (81772938 to L.L., 81872406 and 81630073 to W.Q.G.), State Key Laboratory of Oncogenes and Related Genes (KF01801 to L.L.), Science and Technology Commission of Shanghai Municipality (18140902700 and 19140905500 to L.L., 16JC1405700 to W.Q.G.), KC Wong foundation (to W.Q.G.), 111 project (B21024 to W.Q.G.) and Innovation Research Plan from Shanghai Municipal Education Commission (ZXGF082101 to L.L.), by the Shenzhen Basic Research Foundation (JCYJ20170818090044949), and the Guangdong Province Basic Research Foundation (2018A030310012). The study is also supported by Bio-ID Center, School of Biomedical Engineering, Shanghai Jiao Tong University.

Abbreviations

AMP	antimicrobial peptide
AOM	azoxymethane
7-AAD	7-aminoactinomycin D
CD	Crohn's disease
CRC	colorectal cancer
DSS	dextran sodium sulfate
GO	gene ontology
H2DCFDA	2′,7′-dichlorodihydrofluorescein diacetate
H3K36	histone H3 lysine 36
IBD	inflammatory bowel disease
IEC	intestinal epithelial cell
NAC	N-acetyl-L-cysteine
8-OHdG	8-oxo-2′-deoxyguanosine
PRDX	peroxiredoxin
ROS	reactive oxygen species
RT-qPCR	Real-Time quantitative PCR
UC	ulcerative colitis
ZO-1	tight junction protein 1

Appendix A. Supplementary data

Supplementary data to this article can be found online at https://doi.org/10.1016/j.redox.2021.102004.

References

[1] K.J. Maloy, F. Powrie, Intestinal homeostasis and its breakdown in inflammatory bowel disease, Nature 474 (7351) (2011) 298–306.
[2] A. Kaser, S. Zeissig, R.S. Blumberg, Inflammatory bowel disease, Annu. Rev. Immunol. 28 (2010) 573–621.
[3] A. Mantovani, et al., Cancer-related inflammation, Nature 454 (7203) (2008) 436–444.
[4] S.I. Grivennikov, F.R. Greten, M. Karin, Immunity, inflammation, and cancer, Cell 140 (6) (2010) 883–899.
[5] C.D. Gillen, et al., Ulcerative colitis and Crohn's disease a comparison of the colorectal cancer risk in extensive colitis, Gut 35 (1994) 1590–1592.
[6] R.J. Xavier, D.K. Podolsky, Unravelling the pathogenesis of inflammatory bowel disease, Nature 448 (7152) (2007) 427–434.
[7] M. Rescigno, The intestinal epithelial barrier in the control of homeostasis and immunity, Trends Immunol. 32 (6) (2011) 256–264.
[8] R. Nowarski, et al., Epithelial IL-18 equilibrium controls barrier function in colitis, Cell 163 (6) (2015) 1444–1456.
[9] H. Schmitz, et al., Altered tight junction structure contributes to the impaired epithelial barrier function in ulcerative colitis, Gastroenterology 116 (1999) 301–309.
[10] A.M. Westbrook, A. Szakmary, R.H. Schiestl, Mechanisms of intestinal inflammation and development of associated cancers: lessons learned from mouse models, Mutat. Res. 705 (1) (2010) 40–59.
[11] O.A. Sedelnikova, et al., Role of oxidatively induced DNA lesions in human pathogenesis, Mutat. Res. 704 (1–3) (2010) 152–159.
[12] F.A. Moura, et al., Antioxidant therapy for treatment of inflammatory bowel disease: does it work? Redox Biol 6 (2015) 617–639.
[13] R. Ravindran, et al., The amino acid sensor GCN2 controls gut inflammation by inhibiting inflammasome activation, Nature 531 (7595) (2016) 523–527.
[14] C.W. Barrett, et al., Selenoprotein P influences colitis-induced tumorigenesis by mediating stemness and oxidative damage, J. Clin. Invest. 125 (7) (2015) 2646–2660.

[15] A. Federico, et al., Chronic inflammation and oxidative stress in human carcinogenesis, Int. J. Canc. 121 (11) (2007) 2381–2386.
[16] T. Tian, Z. Wang, J. Zhang, Pathomechanisms of oxidative stress in inflammatory bowel disease and potential antioxidant therapies, Oxid Med Cell Longev 2017 (2017), 4535194.
[17] M. Darnaud, et al., Enteric delivery of regenerating family member 3 alpha alters the intestinal microbiota and controls inflammation in mice with colitis, Gastroenterology 154 (4) (2018) 1009–1023 e14.
[18] J. Kinchen, et al., Structural remodeling of the human colonic mesenchyme in inflammatory bowel disease, Cell 175 (2) (2018) 372–386 e17.
[19] R. Pei, et al., Aronia berry supplementation mitigates inflammation in T cell transfer-induced colitis by decreasing oxidative stress, Nutrients 11 (6) (2019).
[20] M. Liu, et al., BRG1 attenuates colonic inflammation and tumorigenesis through autophagy-dependent oxidative stress sequestration, Nat. Commun. 10 (1) (2019) 4614.
[21] M. Okuda, et al., Mitochondrial injury, oxidative stress, and antioxidant gene expression are induced by hepatitis C virus core protein, Gastroenterology 122 (2) (2002) 366–375.
[22] L. Kruidenier, et al., Intestinal oxidative damage in inflammatory bowel disease: semi-quantification, localization, and association with mucosal antioxidants, J. Pathol. 201 (1) (2003) 28–36.
[23] T. Alenghat, et al., Histone deacetylase 3 coordinates commensal-bacteria-dependent intestinal homeostasis, Nature 504 (7478) (2013) 153–157.
[24] C.V. Theodoris, et al., Human disease modeling reveals integrated transcriptional and epigenetic mechanisms of NOTCH1 haploinsufficiency, Cell 160 (6) (2015) 1072–1086.
[25] M. Albert-Bayo, et al., Intestinal mucosal mast cells: key modulators of barrier function and homeostasis, Cells 8 (2) (2019).
[26] R. Hasler, et al., A functional methylome map of ulcerative colitis, Genome Res. 22 (11) (2012) 2130–2137.
[27] J. Cooke, et al., Mucosal genome-wide methylation changes in inflammatory bowel disease, Inflamm. Bowel Dis. 18 (11) (2012) 2128–2137.
[28] A.S. Wellman, et al., Intestinal epithelial sirtuin 1 regulates intestinal inflammation during aging in mice by altering the intestinal microbiota, Gastroenterology 153 (3) (2017) 772–786.
[29] S. Chakrabarty, et al., Targeted sequencing-based analyses of candidate gene variants in ulcerative colitis-associated colorectal neoplasia, Br. J. Canc. 117 (1) (2017) 136–143.
[30] T.S. Mikkelsen, et al., Genome-wide maps of chromatin state in pluripotent and lineage-committed cells, Nature 448 (7153) (2007) 553–560.
[31] M. Hu, et al., Histone H3 lysine 36 methyltransferase Hypb/Setd2 is required for embryonic vascular remodeling, Proc. Natl. Acad. Sci. U. S. A. 107 (7) (2010) 2956–2961.
[32] S.X. Pfister, et al., Inhibiting WEE1 selectively kills histone H3K36me3-deficient cancers by dNTP starvation, Canc. Cell 28 (5) (2015) 557–568.
[33] Y. Zhang, et al., H3K36 histone methyltransferase Setd2 is required for murine embryonic stem cell differentiation toward endoderm, Cell Rep. 8 (6) (2014) 1989–2002.
[34] N. Kanu, et al., SETD2 loss-of-function promotes renal cancer branched evolution through replication stress and impaired DNA repair, Oncogene 34 (46) (2015) 5699–5708.
[35] F. Li, et al., The histone mark H3K36me3 regulates human DNA mismatch repair through its interaction with MutSalpha, Cell 153 (3) (2013) 590–600.
[36] J. Terzic, et al., Inflammation and colon cancer, Gastroenterology 138 (6) (2010) 2101–2114 e5.
[37] H. Parker, et al., Genomic disruption of the histone methyltransferase SETD2 in chronic lymphocytic leukaemia, Leukemia 30 (11) (2016) 2179–2186.
[38] B.G. Mar, et al., Mutations in epigenetic regulators including SETD2 are gained during relapse in paediatric acute lymphoblastic leukaemia, Nat. Commun. 5 (2014) 3469.
[39] D.M. Walter, et al., Systematic in vivo inactivation of chromatin-regulating enzymes identifies Setd2 as a potent tumor suppressor in lung adenocarcinoma, Canc. Res. 77 (7) (2017) 1719–1729.
[40] J.J. Lee, et al., Tracing oncogene rearrangements in the mutational history of lung adenocarcinoma, Cell 177 (7) (2019) 1842–1857 e21.
[41] L. Wang, et al., H3K36 trimethylation mediated by SETD2 regulates the fate of bone marrow mesenchymal stem cells, PLoS Biol. 16 (11) (2018), e2006522.
[42] Z. Ji, et al., The histone methyltransferase Setd2 is indispensable for V(D)J recombination, Nat. Commun. 10 (1) (2019) 3353.
[43] n. niu, et al., Loss of Setd2 promotes Kras-induced acinar-to-ductal metaplasia and epithelia–mesenchymal transition during pancreatic carcinogenesis, Gut (2019) 1–12, 0.
[44] Q. Xu, et al., SETD2 regulates the maternal epigenome, genomic imprinting and embryonic development, Nat. Genet. 51 (5) (2019) 844–856.
[45] X. Zuo, et al., The histone methyltransferase SETD2 is required for expression of acrosin-binding protein 1 and protamines and essential for spermiogenesis in mice, J. Biol. Chem. 293 (24) (2018) 9188–9197.
[46] S. Wirtz, et al., Chemically induced mouse models of intestinal inflammation, Nat. Protoc. 2 (3) (2007) 541–546.
[47] S. Wirtz, M.F. Neurath, Mouse models of inflammatory bowel disease, Adv. Drug Deliv. Rev. 59 (11) (2007) 1073–1083.
[48] M. Wlodarska, et al., NLRP6 inflammasome orchestrates the colonic host-microbial interface by regulating goblet cell mucus secretion, Cell 156 (5) (2014) 1045–1059.
[49] C.L. Bevins, N.H. Salzman, Paneth cells, antimicrobial peptides and maintenance of intestinal homeostasis, Nat. Rev. Microbiol. 9 (5) (2011) 356–368.
[50] I. Okayasu, et al., A novel method in the induction of reliable experimental acute and chronic ulcerative colitis in mice, Gastroenterology 98 (1990) 694–702.
[51] J. Gupta, et al., Dual function of p38alpha MAPK in colon cancer: suppression of colitis-associated tumor initiation but requirement for cancer cell survival, Canc. Cell 25 (4) (2014) 484–500.
[52] V. Ramirez-Carrozzi, et al., IL-17C regulates the innate immune function of epithelial cells in an autocrine manner, Nat. Immunol. 12 (12) (2011) 1159–1166.
[53] J.W. Steinke, L. Borish, 3. Cytokines and chemokines, J. Allergy Clin. Immunol. 117 (2 Suppl Mini-Primer) (2006) S441–S445.
[54] H. Cha, et al., Increased susceptibility of IDH2-deficient mice to dextran sodium sulfate-induced colitis, Redox Biol 13 (2017) 32–38.
[55] P. Patel, S. Chatterjee, Peroxiredoxin6 in endothelial signaling, Antioxidants 8 (3) (2019).
[56] Y. Belkaid, T.W. Hand, Role of the microbiota in immunity and inflammation, Cell 157 (1) (2014) 121–141.
[57] S. Rakoff-Nahoum, et al., Recognition of commensal microflora by toll-like receptors is required for intestinal homeostasis, Cell 118 (2) (2004) 229–241.
[58] A. Morgun, et al., Uncovering effects of antibiotics on the host and microbiota using transkingdom gene networks, Gut 64 (11) (2015) 1732–1743.
[59] G. Ray, M.S. Longworth, Epigenetics, DNA organization, and inflammatory bowel disease, Inflamm. Bowel Dis. 25 (2) (2019) 235–247.
[60] A.M. Fontebasso, et al., Mutations in SetD2 and genes affecting histone H3K36 methylation target hemispheric high-grade gliomas, Acta Neuropathol. 125 (2013) 659–669.
[61] F. Neri, et al., Intragenic DNA methylation prevents spurious transcription initiation, Nature 543 (7643) (2017) 72–77.
[62] Z.L. Piedra-Quintero, et al., Myosin 1F regulates M1-polarization by stimulating intercellular adhesion in macrophages, Front. Immunol. 9 (2018) 3118.
[63] C. Serrano, et al., Compartmentalized response of IL-6/STAT3 signaling in the colonic mucosa mediates colitis development, J. Immunol. 202 (4) (2019) 1239–1249.
[64] I.Y. Park, et al., Dual chromatin and cytoskeletal remodeling by SETD2, Cell 166 (4) (2016) 950–962.
[65] K. Chen, et al., Methyltransferase SETD2-mediated methylation of STAT1 is critical for interferon antiviral activity, Cell 170 (3) (2017) 492–506 e14.